ARTICLES
PUBLISHED ONLINE: 16 MARCH 2014 | DOI: 10.1038/NGEO2101
nature geoscience

Surface-water iron supplies in the Southern Ocean sustained by deep winter mixing

Alessandro Tagliabue[1,2*], Jean-Baptiste Sallée[3,4,5], Andrew R. Bowie[6], Marina Lévy[3,4], Sebastiaan Swart[2,7] and Philip W. Boyd[8,9]

Low levels of iron limit primary productivity across much of the Southern Ocean. At the basin scale, most dissolved iron is supplied to surface waters from subsurface reservoirs, because land inputs are spatially limited. Deep mixing in winter together with year-round diffusion across density surfaces, known as diapycnal diffusion, are the main physical processes that carry iron-laden subsurface waters to the surface. Here, we analyse data on dissolved iron concentrations in the top 1,000 m of the Southern Ocean, taken from all known and available cruises to date, together with hydrographic data to determine the relative importance of deep winter mixing and diapycnal diffusion to dissolved iron fluxes at the basin scale. Using information on the vertical distribution of iron we show that deep winter mixing supplies ten times more iron to the surface ocean each year, on average, than diapycnal diffusion. Biological observations from the sub-Antarctic sector suggest that following the depletion of this wintertime iron pulse, intense iron recycling sustains productivity over the subsequent spring and summer. We conclude that winter mixing and surface-water iron recycling are important drivers of temporal variations in Southern Ocean primary production.

The micronutrient iron is an important regulator of primary productivity and therefore the strength of the biological carbon pump in the Southern Ocean[1,2]. This region is of key importance to both the global carbon cycle and air–sea carbon dioxide fluxes[3,4] and the impact of future or past climate variability is mediated to a large degree by modifications to Fe supply to the biota[5]. Despite a marked expansion of dissolved Fe (DFe $\leq 0.2\,\mu m$) observations in the 'GEOTRACES' era[6] and several investigations[7,8] into the magnitude of exogenous inputs of DFe, little attention has been focussed on the physical processes that supply DFe at the basin-scale from subsurface reservoirs, enriched in DFe from both external inputs[1,8] and remineralization[9]. In general, wintertime deep mixing (or entrainment), year-round vertical diapycnal diffusion and Ekman upwelling/downwelling are the major physical processes involved in the vertical supply of DFe to phytoplankton[10–12]. The maximum depth of mixing over the year (MLD_{MAX}) and the DFe inventory within this stratum control the degree of DFe entrainment. Diapycnal diffusion depends on the vertical diffusivity (k_z) and the vertical DFe gradient at the base of the MLD ($\partial DFe/\partial z_{MLD}$), whereas the Ekman upwelling/downwelling of DFe depends on the wind stress curl and the concentration of DFe at the base of the mixed layer. In terms of their drivers, entrainment is primarily controlled by air–sea surface buoyancy fluxes, whereas Ekman upwelling/downwelling responds to momentum forcing from winds, and near-surface diapycnal diffusion extracts its energy from a range of sources, including winds and buoyancy. As each of these factors will be differentially altered by climate change[5,13], understanding the climate sensitivity of vertical DFe supply to Southern Ocean phytoplankton depends on the relative role played by different physical input pathways. Despite previous attempts[10,11], the importance of each physical pathway is poorly quantified owing to historically sparse data coverage, and this shortcoming hampers efforts to constrain the response of Southern Ocean biogeochemical cycling to climate change.

A key influence on the vertical input of DFe to the mixed layer is exerted by its water column profile and, in particular, the location and magnitude of vertical concentration gradients ($\partial Fe/\partial z$). The depth at which $\partial Fe/\partial z$ is maximal is termed the 'ferricline' (hereafter: Z_{Fe}, Supplementary Fig. 1), and as for nitrate (and the 'nitracline'), is critical in understanding how changes in winds and buoyancy fluxes will impact physical DFe supply processes. Like nitrate stocks in the North Atlantic, DFe concentrations are typically depleted (not necessarily to zero) in Southern Ocean surface waters during spring/summer[6] owing to biological consumption and prevailing DFe limitation[14], with greater subsurface concentrations from organic matter remineralization. However, unlike nitrate, Fe is also lost from the dissolved pool as a result of particle scavenging, has important subsurface inputs from ocean sediments and hydrothermal vents[1,8] and is probably remineralized more slowly[15,16], such that Z_{Fe} can be deeper than both the nitracline and MLD (refs 15,17–19). However, the nature of the depth offset between Z_{Fe} and MLD across the wider Fe-limited Southern Ocean and its relation to physical DFe supply processes remains uncertain. If Z_{Fe} were to be consistently deeper than the MLD at basin scales, this would have important implications for the

[1]Department of Earth, Ocean and Ecological Sciences, School of Environmental Sciences, University of Liverpool, Liverpool, L69 3GP, UK, [2]Southern Ocean Carbon and Climate Observatory, CSIR, Stellenbosch 7599, South Africa, [3]Sorbonne Universités, UPMC Univ., Paris 06, UMR 7159, LOCEAN-IPSL, F-75005, Paris, France, [4]CNRS, UMR 7159, LOCEAN-IPSL, F-75005, Paris, France, [5]British Antarctic Survey, High Cross, Cambridge, CB3 0ET, UK, [6]Antarctic Climate and Ecosystems CRC, University of Tasmania, Private Bag 80, Hobart, Tasmania 7001, Australia, [7]Department of Oceanography, Marine Research Institute, University of Cape Town, Rondebosch 7701, South Africa, [8]NIWA Centre of Chemical and Physical Oceanography, Department of Chemistry, University of Otago, Dunedin 9016, New Zealand, [9]Institute for Marine and Antarctic Studies, University of Tasmania, Private Bag 129, Hobart, Tasmania 7001, Australia. *e-mail: a.tagliabue@liverpool.ac.uk

magnitude of vertical DFe supply and its seasonal variability, highlighting the unique nature of Fe cycling. Here we use a new approach that synthesizes recent DFe observations (including recent GEOTRACES field campaigns)[6], co-localized MLDs from the Argo float archive[20] and satellite phytoplankton Fe utilization estimates[7] (Methods) for the first time to quantify the processes responsible for the seasonal supply of DFe in the Southern Ocean. Our goals were to document Z_{Fe} depths, their relation to MLDs and to quantify the spatial variability in the supply of DFe from entrainment, diapycnal mixing and Ekman upwelling/downwelling across the Southern Ocean.

Ferricline depth and quantifying vertical iron supply

Owing to its fundamental role in regulating DFe inputs, we first determined Z_{Fe} across the Southern Ocean. The mean depth of Z_{Fe} was 333 m (median of 350 m) across the 140 unique determinations (Fig. 1a). Much of the variability in Z_{Fe} in absolute depth is eliminated when the potential density anomaly (σ_θ, kg m^{-3}; referenced at the ocean surface) at the depth of Z_{Fe} is plotted (determined from Argo profiling floats; Fig. 1b). Consistent across all sampled Southern Ocean sectors, we find that Z_{Fe} is typically associated with denser waters south of the Polar Front ($\sigma_\theta >$ 27.5 kg m^{-3}) and with lighter waters ($\sigma_\theta <$ 27.5 kg m^{-3}) further north, with a striking decline in σ_θ at Z_{Fe} from south to north (Fig. 1b). Because σ_θ declines at any depth from south to north, modifications to isopycnal depths are a likely driver of a large part of the variability in the absolute depth of Z_{Fe} (Fig. 1, especially at relatively adjacent locations), probably following some 'preconditioning' from Fe-specific biogeochemical processes (encapsulated by longer remineralization length scales[15]). The vertical gradient at Z_{Fe} (∂Fe/∂z_{ZFe}) is generally much greater than that at the MLD (∂DFe/∂z_{MLD}), which indicates that Z_{Fe} is the most significant vertical gradient in the upper 1,000 m (Supplementary Fig. 2). Moreover, ∂DFe/∂z_{ZFe} is greatest (meaning a 'sharper' ferricline) in the South Atlantic sector, indicating the signature of DFe subsurface lateral transfer from numerous regional islands[1,7] in the DFe profiles. On average, Z_{Fe} is deeper than the co-located MLD by 245 m (median = 210 m; Fig. 2a), with no seasonal bias where data are available (Fig. 1c). As a measure of MLD variability, the offset changes to 199 m or 288 m using MLDs at $+2\sigma$ or -2σ, respectively (see Methods for details on the computation of the standard deviation, σ). Thus, irrespective of the time of year, we demonstrate that Z_{Fe} is robustly and significantly deeper than the MLD across much of the Southern Ocean. That nitracline and phosphocline depths are more closely coupled to the MLD illustrates unique behaviour of DFe in this regard (Supplementary Fig. 3).

That Z_{Fe} is almost always much deeper than the concomitant MLD indicates limited input of DFe from diapycnal diffusion due to weak ∂Fe/∂z_{MLD} (Supplementary Fig. 2b). For example, applying typical Southern Ocean k_z values[18,21–23] of 10^{-5}–10^{-4} m^2 s^{-1} results in 1.6–15.7 nmol DFe m^{-2} d^{-1} from diapycnal diffusion input. Across all combinations of MLD and k_z (that is, $\pm2\sigma$ for MLD and 10^{-5}–10^{-4} m^2 s^{-1} for k_z), diapycnal diffusion is 0.25–7.7 μmol DFe m^{-2} yr^{-1} (Fig. 2b; consistent with estimates from occasional *in situ* studies[14,16,17,24]). The highest rates of diapycnal diffusion DFe input are found near the Antarctic Peninsula and are comparable to recent regional observations[24]. However, such values do not seem generally representative of the offshore Southern Ocean, where diapycnal diffusion inputs of < 0.2 μmol DFe m^{-2} yr^{-1} generally prevail (Fig. 2b).

In contrast to diapycnal diffusion, the winter entrainment pulse can supply much more DFe. Entrainment is quantified using winter mixed-layer depths (MLD_{MAX}) from Argo profiles, alongside estimated winter Z_{Fe} (Z_{FeMAX}, see Methods). Whereas winter mixing depths exceed Z_{FeMAX} more often, the mean offset remains 212 m (median = 143 m; Fig. 2a), similar to the sole winter DFe section[25].

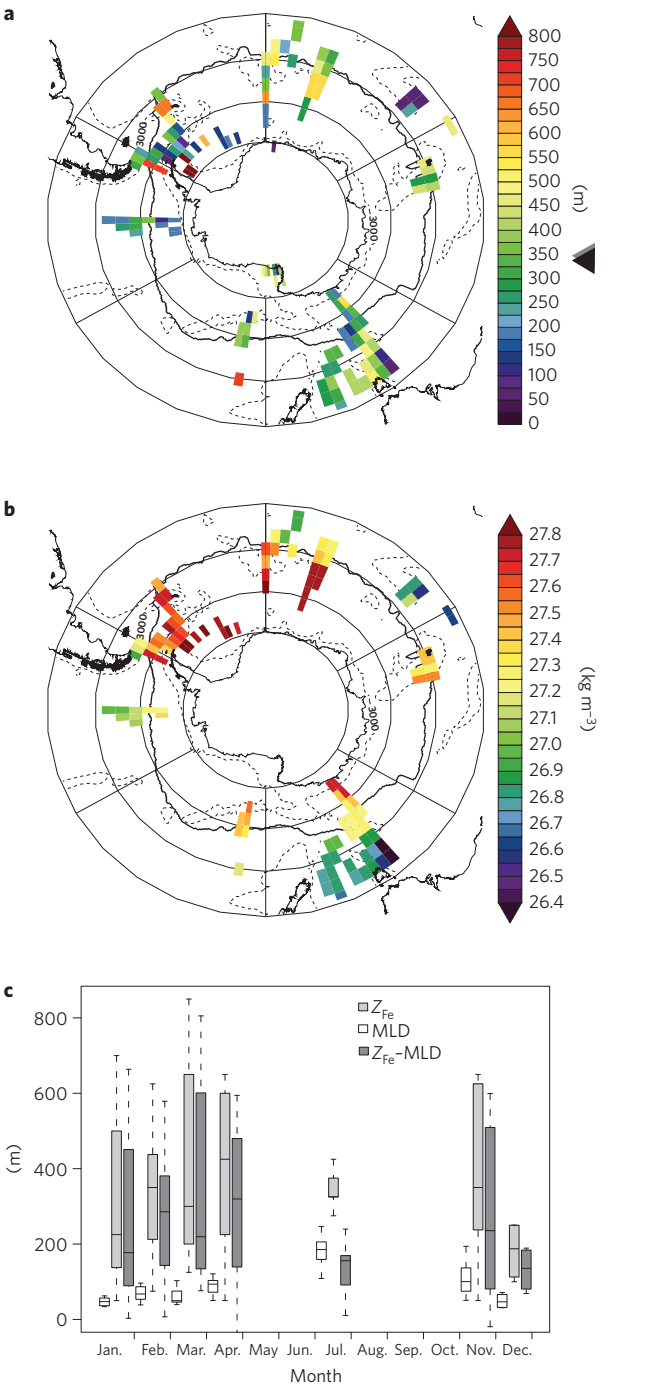

Figure 1 | Depths and potential density of the ferricline and its seasonal evolution. a, The depth of the ferricline (m); black and grey triangles denote the mean and median, respectively. **b**, Potential density anomaly (σ_θ, kg m^{-3}) associated with the ferricline depth. **c**, Box and whisker plots of the seasonal cycle in MLD, Z_{Fe} and Z_{Fe}-MLD (the box represents the quartiles 1–3, with the vertical bar corresponding to the median and the whiskers representing 1.5 times the inter quartile range). Although calculations for **a** and **b** are performed on a 1° grid, they are shown using a 3° grid for clarity. The 3,000 m isobath and the mean Polar Front position (black line[6]) are also shown.

At $\pm2\sigma$ on MLD_{MAX}, mean offsets are 114 m and 311 m. To correctly compute net entrainment inputs also requires a consideration of the DFe stocks that are detrained during springtime mixed-layer shallowing, which can be estimated using Argo profiling data at each

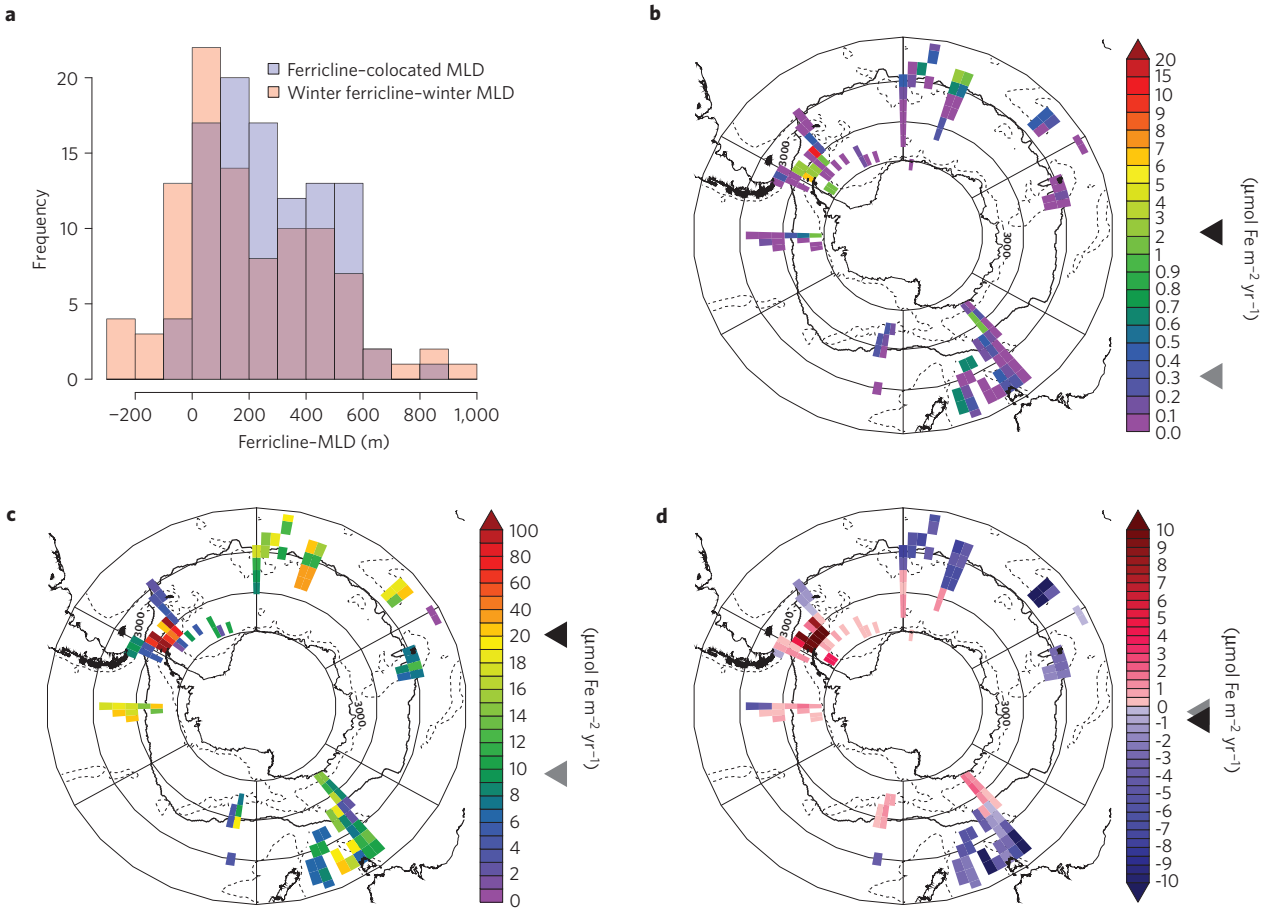

Figure 2 | The relationship between the ferricline and mixed-layer depths and calculations of physically mediated iron fluxes. **a**, Histogram of the offset (m) between the depth of the ferricline and the mixed-layer depth (lilac and peach for concomitant and winter MLDs, respectively; purple indicates overlap). **b**, Annual diapycnal diffusion flux of Fe across the mixed layer (μmol m^{-2} yr^{-1}). **c**, Annual entrainment flux of Fe (μmol m^{-2} yr^{-1}). **d**, Annual Ekman DFe term (μmol m^{-2} yr^{-1}), with negative/positive values indicating downwelling/upwelling of DFe. In **b**–**d**, black and grey triangles denote the mean and median, respectively. Gridding for **b**–**d** is as for Fig. 1a.

DFe profile location. Ultimately, the mean entrainment Fe input is 21.1 μmol DFe m^{-2} yr^{-1} (or 9.5–33.2 μmol DFe m^{-2} yr^{-1} at $\pm 2\sigma$ on MLD_{MAX}). This is more than ten times greater (on average) than the annual diapycnal diffusion inputs estimated above. Spatially (Fig. 2c), entrainment inputs are higher than average around the Antarctic Peninsula and some parts of the Indian and Pacific sectors of the Southern Ocean. Much lower entrainment fluxes are present in many other regions owing to weak vertical gradients in DFe persisting down to MLD_{MAX}. That appreciable entrainment fluxes of DFe arise despite ~200 m offsets persisting between Z_{FeMAX} and MLD_{MAX}, highlights the smaller vertical gradients in DFe at the top of the ferricline (but shallower than Z_{FeMAX}) that are captured by winter mixing.

Ekman upwelling and downwelling is computed using DFe concentrations at the mixed-layer base and the wind stress curl (Fig. 2d). Ekman fluxes are strongly dependent on latitude, switching from net losses to gains of DFe as the sign of the wind stress curl changes across the atmospheric subtropical jet (Fig. 2d). In general, Ekman fluxes are comparable to those associated with diapycnal diffusion, rather than entrainment, and on average are a slight net loss of DFe from the system (−0.7 μmol DFe m^{-2} yr^{-1} or a median of −0.4 μmol DFe m^{-2} yr^{-1}), although this is probably sensitive to the sampling frequency north and south of the atmospheric subtropical jet. Finally, transient MLD deepening during the phytoplankton growth season might entrain additional Fe, but using the rate of change in the MLD from Argo floats ten days either side of the sampling date, we found this process to be negligible.

Additional regional or localized sources of DFe to the mixed layer are provided from dust deposition[26] and melting of sea ice[27], icebergs[28,29] or glaciers[29,30]. Estimates of their supply rates are difficult to generalize as they are usually derived from models or point-source observations that are not easily extrapolated to basin scales. Upper limits[7] for dust deposition, sea ice melting and icebergs are on the order of 20 μmol DFe m^{-2} yr^{-1}, making them comparable to entrainment. However, it is notable that many of these additional DFe fluxes are extremely localized[7] and these upper limits will only be realized close to sources (that is, nearshore waters). Therefore over much of the offshore Southern Ocean that is the focus of this study, their contribution to DFe supply will be greatly reduced. The major basin-scale role we find for entrainment is similar to a recent study conducted at one station in the, oceanographically very different, western North Pacific[31].

Iron supply and utilization

We now consider how diapycnal diffusion and entrainment DFe sources can meet estimates of biological Fe utilization. Basin-scale quantifications of phytoplankton Fe utilization rely on combining estimates of net primary production with algal Fe utilization from laboratory culture experiments[7]. Direct comparison with our physical input terms is complicated, as much of the Fe utilization is met from recycled Fe, illustrated by *f*e-ratios (proportion of

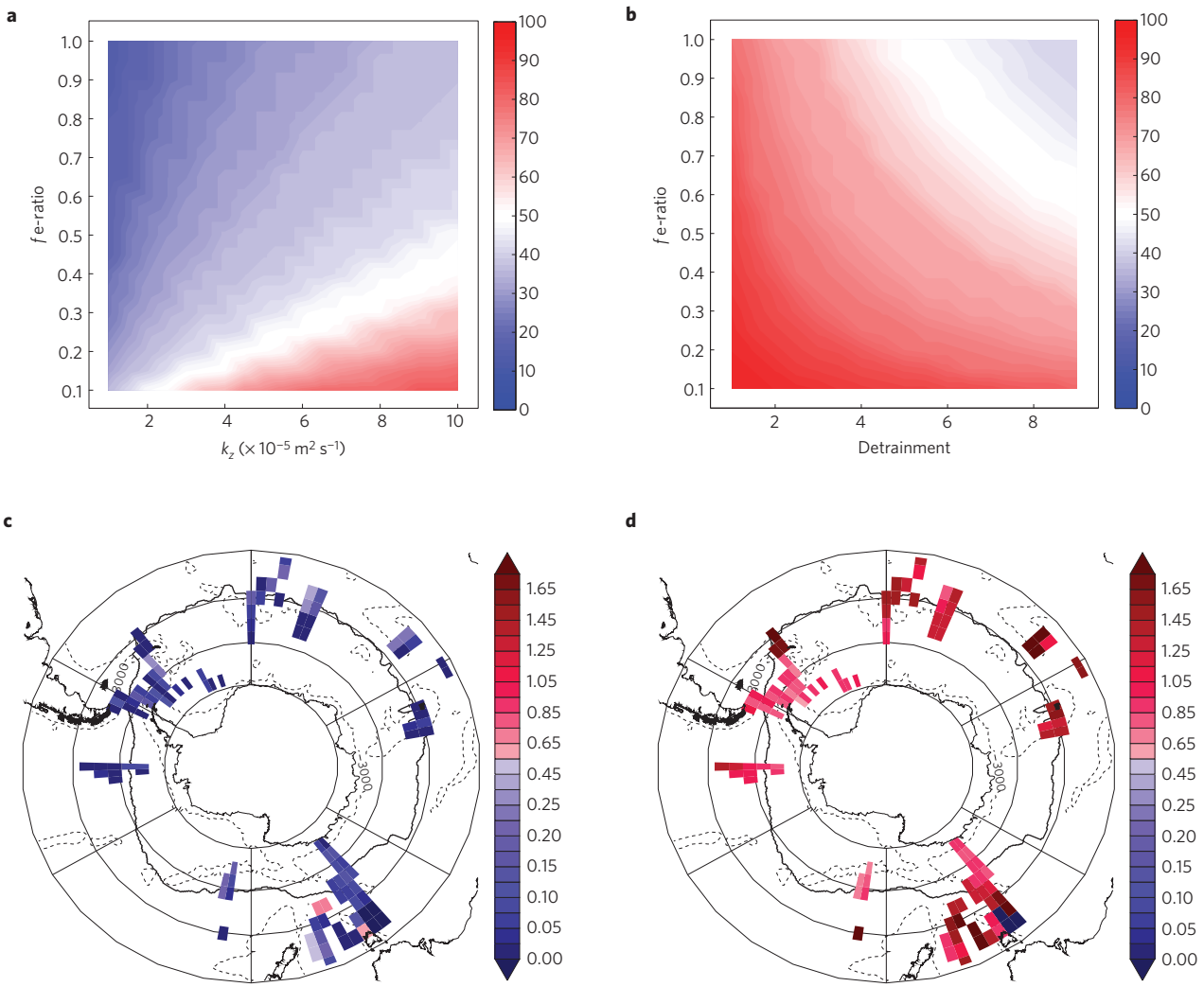

Figure 3 | Assessments of how different physically mediated iron supply mechanisms compare to utilization and their contribution to total iron fluxes. **a**, Percentage of locations where diapycnal diffusion can match iron utilization over different scenarios regarding the *f* e-ratio and k_z. **b**, Percentage of locations where entrainment can match iron utilization over different scenarios regarding the *f* e-ratio and detrainment. **c**,**d**, Proportional contribution of diapycnal diffusion (**c**) and entrainment (**d**) to total physical DFe supply (see also Supplementary Fig. 3b). Gridding for **c** and **d** is as for Fig. 1a.

Fe uptake from 'new' sources[17]) that range between 0.06 and 0.5 from low- to high-DFe waters[14,16,17,32]. Moreover, phytoplankton represent only about half of total Fe utilization associated with microbial and metazoan assemblages[1]. Last, the quantification of diapycnal diffusion and entrainment are sensitive to assumptions regarding k_z and (to a lesser extent) the degree of detrainment, respectively. Nevertheless, by exploring the plausible parameter space for the *f* e-ratio, k_z and detrainment we can assess the capacity for diapycnal diffusion and entrainment to meet phytoplankton Fe utilization (where DFe data are presently available). When k_z is low, diapycnal diffusion cannot match utilization in >50% of locations, regardless of *f* e-ratios (Fig. 3a). Even when k_z approaches its upper limit of 10^{-4} m^2 s^{-1}, diapycnal diffusion meets utilization in >50% of cases only when the *f* e-ratio reaches unrealistically low levels (that is minimal reliance on new Fe, Fig. 3a). In contrast, it is only when the detrainment term is greatest (approximately three times higher than the Argo float data average of 3.1) and the *f* e-ratio is maximal (that is, has the greatest reliance on new Fe) that entrainment cannot meet utilization in >50% of cases (Fig. 3b). As more DFe data are collected in the offshore Southern Ocean then the importance of diapycnal diffusion will probably further decline. When examined spatially, even in locations where diapycnal diffusion is strong (for example, near the Antarctic Peninsula, Fig. 2b), it provides only ~10–20% of total DFe inputs from physically mediated fluxes (Fig. 3c). In contrast, entrainment always provides >60% of total DFe input (Fig. 3d) and is often able to offset regional losses of DFe due to Ekman downwelling (Fig. 2d). Thus, it seems diapycnal diffusion is rarely a significant component of seasonal DFe supply in the Southern Ocean, which we suggest is dominated by a 'one-off' pulse of new DFe from winter entrainment. It is noteworthy in this context that entrainment can always match available estimates of iron utilization (Supplementary Methods).

Our results permit an illustration of the key processes involved in the supply and cycling of DFe over the Southern Ocean phytoplankton growth season (Fig. 4). Deep winter mixing maximizes access to subsurface DFe reservoirs and re-stocks the mixed layer. During spring, this inventory is depleted rapidly (days to weeks) by both the upper ocean biota[14] and abiotic scavenging onto settling particles. Diapycnal diffusion will therefore become the major DFe supply term from late spring onwards, but its low rates (~7–21 nmol DFe m^{-2} d^{-1}) cannot be reconciled with measured mixed-layer phytoplankton utilization[14,16,17,32,33] of approximately 2–6 μmol DFe m^{-2} d^{-1}. Phytoplankton are therefore heavily

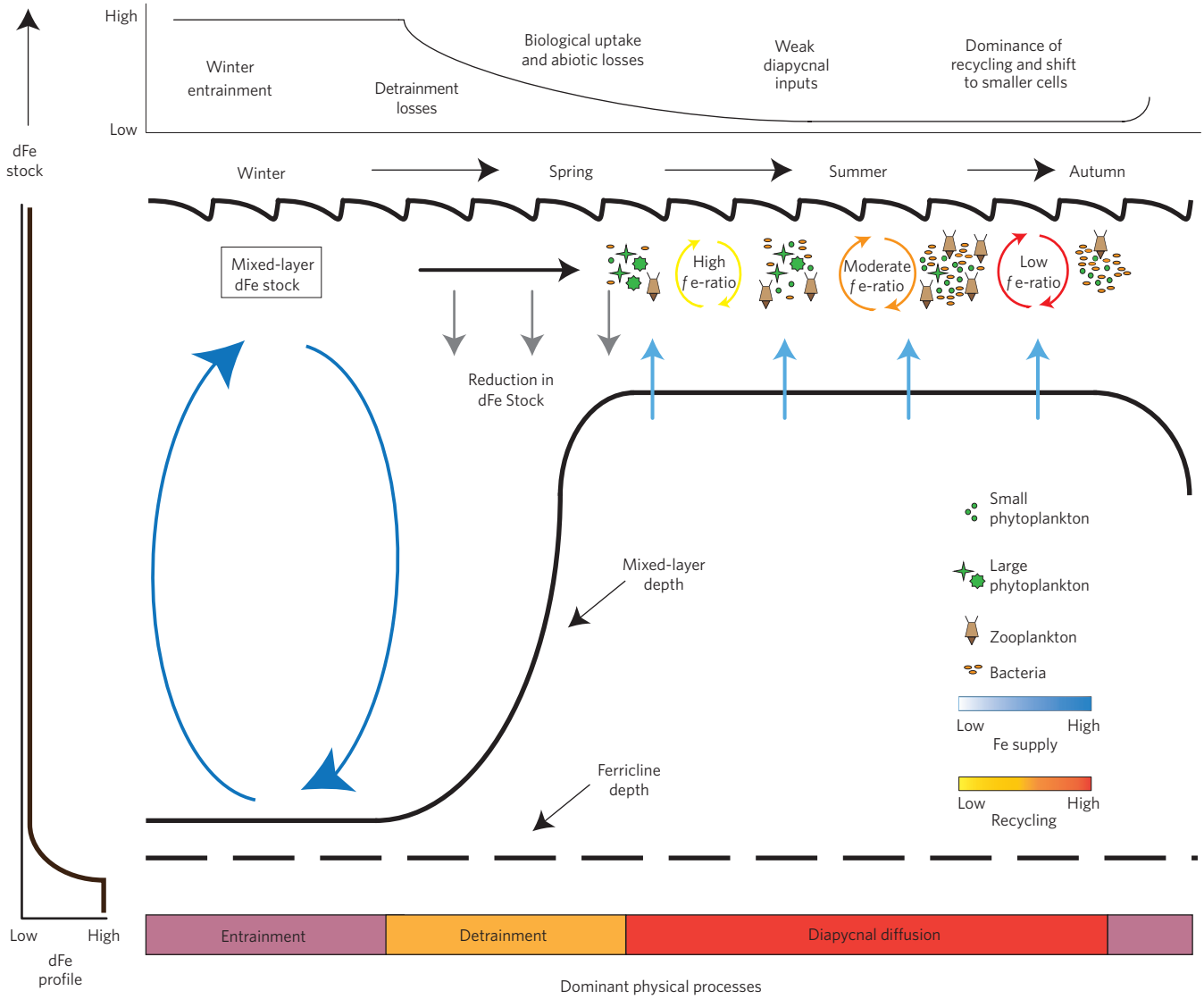

Figure 4 | A schematic representation of the seasonal variability in Southern Ocean Fe cycling. We emphasize seasonal changes in the physical supply of Fe (blue arrows), mixed-layer depth and the mixed-layer DFe inventory, as well as the magnitude of recycling (yellow, orange and red arrows) and pelagic community composition. The dominant physical processes over the season is conceptualized at the bottom of the figure. We note that some recycling probably occurs below the mixed layer and can be entrained the following winter.

reliant on DFe from pelagic recycling, with *f*e-ratios declining accordingly over summer[14]. This highlights the importance of the 'ferrous wheel'[33] in late spring and summer, when DFe inputs to the mixed layer are weak. Indeed, measured Fe regeneration rates of 5–10 μmol m^{-2} d^{-1} more closely match phytoplankton requirements[14]. We suggest that an increasing importance of recycled Fe due to low diapycnal diffusion inputs would cause a shift from initially high *f*e-ratios to lower *f*e-ratios over the year. This may prove disadvantageous to larger phytoplankton, such as diatoms, and favour smaller phytoplankton cells[14]. The relative magnitudes of winter DFe replenishment of the mixed layer by entrainment and ongoing diapycnal diffusion is mediated by the degree of coupling between Z_{Fe} and the MLD over the year (for example, Figs 1c, 2a). However, owing to the persistent offsets between Z_{Fe} and the MLD (Fig. 2a), winter entrainment dominates DFe supply over much of the Southern Ocean (Fig. 3d), with little vertical DFe input to the biota from spring onwards (Fig. 4). This emphasizes the role of Fe recycling by herbivory, bacterivory and virally-mediated microbial mortality in regulating the mixed-layer DFe pool until the mixed layer deepens again in autumn. Accordingly, better understanding the dynamics of DFe turnover rates and the associated bioavailability of recycled DFe would be an important future focus.

Our conceptual model posits that because Z_{Fe} is so deep, recycling is crucial in maintaining mixed-layer DFe stocks following the pulse of DFe from entrainment (Fig. 4). The detailed biological rate data supporting this view has been obtained from detailed process studies conducted in the sub-Antarctic zone of the Southern Ocean[15–17,32,33]. Turning to the silicate-rich waters of the Antarctic zone, our analysis suggests that the paradigm of significant winter entrainment input of DFe followed by little subsequent 'irrigation' from diapycnal iron supply is also true (Fig. 3c,d). But, in addition to Fe recycling, it is also plausible that additional biological factors might influence the seasonal cycle of biological productivity south of the Polar Front in the Antarctic zone. For example, heavily-silicified diatoms are more common here, and their 'luxury uptake' of DFe (refs 34,35) early in the spring (when mixed-layer DFe stocks remain high) may help sustain diatom cell division once this wintertime DFe pulse has been depleted. Nevertheless, any further region-specific processes, such as luxury uptake of iron, would only serve to complement recycling

as a key determinant of phytoplankton growth once the influence of entrained iron ceases in spring/summer (Fig. 4).

Implications for Southern Ocean carbon cycling

DFe regulates phytoplankton growth throughout the Southern Ocean[1,2], hence basin-scale fluctuations in Southern Ocean primary productivity[36] should be linked to changing DFe inputs. Our initial results would suggest an important role for entrainment, as mediated by winter mixing in this context (Fig. 3d). Indeed, using a scale analysis we find inter-annual variation in DFe supply from entrainment is 9.1–33 $\mu mol\,m^{-2}\,yr^{-1}$, as compared to 1.2–3.6 or −1.9–0.4 $\mu mol\,m^{-2}\,yr^{-1}$ from diapycnal diffusion or Ekman, respectively. Inter-annual modifications to dust deposition[37,38] or the melting of sea ice[39] might also be important locally (perhaps ranging by a factor between two and eight[7]), but these inputs cannot readily be extrapolated to basin scales. Inter-annual basin-scale changes in Southern Ocean primary production can at present be assessed only by satellite and are estimated[36] at ∼±11% (from 1997 to 2006). This variability is relatively small in contrast to the large changes in wintertime DFe inputs we estimate and the widely demonstrated role DFe supply plays in setting regional productivity[2]. Robust attribution of causality to the driver(s) of observed fluctuations in remotely-sensed basin-scale primary productivity is so far lacking for the Southern Ocean[36]. Such attribution may be further masked by the unique bio-optical properties of Southern Ocean waters, which probably hinder the utility of remotely sensed productivity datasets[40]. Satellite estimates may be further confounded by the complicated inter-play between physical DFe supply, external DFe inputs and physiological plasticity in phytoplankton DFe utilization[7]. Nevertheless, our results show winter entrainment is pivotal to regional DFe supply and must be part of a future appraisal of the sensitivity of Southern Ocean productivity to basin-scale environmental fluctuations, which has been overlooked in previous assessments[36,41].

Properly accounting for the role of winter entrainment DFe inputs requires the parallel consideration of winter mixing depths and their connection to subsurface DFe reservoirs (Fig. 2a). An improved understanding of the distribution of ferricline depths across the Southern Ocean, as part of the GEOTRACES programme, and how they change on seasonal scales would permit a more widespread identification of regions where entrainment dominates. This would, in turn, highlight locations where primary productivity might be more sensitive to variability in buoyancy fluxes rather than winds. In addition, appraising the sensitivity of Fe recycling to environmental factors on seasonal scales is also crucial as it is clearly the major resupply process over spring–summer once entrainment ceases, with probable implications for ecosystem structure (Fig. 4). Finally, climate models seeking to represent the evolution of the Southern Ocean carbon cycle or productivity[42–46] must pay careful attention to their representation of vertical distributions of DFe. The degree of coupling between Z_{Fe} and the MLD in the model will dictate the relative roles played by different physical DFe supply mechanisms, as well as the importance of mixed-layer recycling of Fe in sustaining productivity over seasonal and inter-annual periods.

Methods

A global DFe database[6] was re-gridded into 1° × 1° longitude and latitude bins (south of 40° S) by month of sampling and on a depth axis with a 25 m resolution in the upper 1,000 m. The compiled Fe profiles were scrutinized in a number of ways. We first required there to be at least one observation shallower than 50 m, one observation deeper than 500 m and at least five observations in total per profile. The remaining profiles were then interpolated on the vertical axis (Supplementary Methods) to determine Z_{Fe}. We decided on the most objective definition possible for Z_{Fe}, that is, the depth at which the $\partial DFe/\partial z$ gradient was maximal (see also: ref. 18), which avoided assigning a subjective threshold concentration. Alternative methods might be imagined that would allow the capturing of the 'top' and 'bottom' of the ferricline using deviations in $\partial DFe/\partial z$ from zero (Supplementary Fig. 1), however they are not easily applied with confidence to such a large dataset. As such our work identifies the 'core' of the ferricline. To avoid deep ocean gradients associated with point sources (for example, hydrothermal vents) being misidentified as the upper ocean ferricline we restricted our analysis to the upper 1,000 m, where hydrothermal tracers show minimal gradients[8]. Finally, because in coastal systems Z_{Fe} might be very close to the seabed owing to sediment input, we decided to remove data where Z_{Fe} was more than 80% of the bottom depth. The total number of unique determinations was 140 or by month: 25 in January, 18 in February, 14 in March, 46 in April, 10 in July, 2 in October, 20 in November and 5 in December. The DFe dataset used in this study is archived and updated here: http://pcwww.liv.ac.uk/~atagliab/LIV_WEB/Data.html.

We calculated the MLD for every Southern Ocean profile with a surface-density difference criterion of $\Delta\sigma_\theta \leq 0.03\,kg\,m^{-3}$ (refs 47,48; Supplementary Fig. 1d). The correspondence between Z_{Fe} and MLD was then examined by co-locating MLDs from either *in situ* CTD profiles and/or Argo profiles[20] (Supplementary Fig. 2d) for the same month and year within 2.5 degrees of a Z_{Fe} determination and weighted by $1/d^4$ (where d is the distance from the Z_{Fe} determination). We also use the maximum MLDs associated with each location for the specific year. Uncertainty in each MLD determination is assessed using a climatology at ±2 s.d.

Diapycnal input is calculated by taking $\partial DFe/\partial z$ at the MLD (Supplementary Fig. 2b) from Argo and multiplying by an estimate of vertical diffusivity (k_z, see main text). Winter entrainment is computed by integrating DFe down to the MLD_{MAX} from Argo. The proportion of the DFe stock entrained in the ML during winter that is detrained during springtime mixed-layer shallowing can be estimated using the MLD_{MAX}:MLD_{MIN} ratio from Argo at each DFe profile location (average = 3.16 ± 1.86, see Supplementary Fig. 2c for a representation of this term). Finally, the Ekman upwelling/downwelling of DFe requires the mean mixed-layer DFe from DFe observations and Argo profiles alongside the wind stress curl. For windstress we used the Quick Scatterometer Mean Wind Field (QuickSCAT MWF) gridded product (this global half-degree-resolution product is processed and distributed by the Centre European Remote Sensing Satellite (ERS) d'Archivage et de Traitement (CERSAT); available online at http://www.ifremer.fr/cersat/). We used weekly maps of wind stress between 1999 and 2009 to produce monthly mean maps over a period consistent with the Argo data. The stated error of the product is less than 7×10^{-3} Pa over the area studied.

To estimate Z_{FeMAX}, we used the robust relationship between Z_{Fe} and density (Fig. 1b), and as Z_{Fe} is below the diabatic surface layer for most profiles we determined Z_{FeMAX} by assuming that Z_{Fe} conserves its density. Thus the change in the density profile between the time of measurement and the time of MLD_{MAX} drives the 'winter' DFe profile. The resulting profiles are illustrated for four case study regions in Supplementary Fig. 4.

The iron utilization estimates combine regionally optimized NPP determinations from ocean colour[36] with estimates of the biogeography in algal Fe/C ratios to arrive at annual Fe utilization estimates (1996–2007). The algal Fe/C ratios are applied using laboratory data from Southern Ocean isolates[7,49]. For reference, the median annual Fe utilization map from ref. 7 is reproduced in Supplementary Fig. 5a.

Received 11 September 2013; accepted 24 January 2014; published online 16 March 2014

References

1. Boyd, P. W. & Ellwood, M. J. The biogeochemical cycle of iron in the ocean. *Nature Geosci.* **3,** 675–682 (2010).
2. Moore, C. M. *et al.* Processes and patterns of oceanic nutrient limitation. *Nature Geosci.* **6,** 701–710 (2013).
3. Sarmiento, J. L., Hughes, T. M. C., Stouffer, R. J. & Manabe, S. Simulated response of the ocean carbon cycle to anthropogenic climate warming. *Nature* **393,** 245–249 (1998).
4. Takahashi, T. *et al.* Climatological mean and decadal change in surface ocean pCO_2, and net sea–air CO_2 flux over the global oceans. *Deep-Sea Res. II* **56,** 554–577 (2009).
5. Boyd, P. W. *et al.* Climate-mediated changes to mixed-layer properties in the Southern Ocean: Assessing the phytoplankton response. *Biogeosciences* **5,** 847–864 (2008).
6. Tagliabue, A. *et al.* A global compilation of dissolved iron measurements: Focus on distributions and processes in the Southern Ocean. *Biogeosciences* **9,** 2333–2349 (2012).
7. Boyd, P. W., Arrigo, K. R., Strzepek, R. & van Dijken, G. L. Mapping phytoplankton iron utilization: Insights into Southern Ocean supply mechanisms. *J. Geophys. Res.* **117,** C06009 (2012).
8. Tagliabue, A. *et al.* Hydrothermal contribution to the oceanic dissolved iron inventory. *Nature Geosci.* **3,** 252–256 (2010).

9. Boyd, P. W., Ibisanmi, E., Sander, S. G., Hunter, K. A. & Jackson, G. A. Remineralization of upper ocean particles: Implications for iron biogeochemistry. *Limnol. Oceanogr.* **55,** 1271–1288 (2010).
10. Moore, J. K., Doney, S. C., Glover, D. M. & Fung, I. Y. Iron cycling and nutrient-limitation patterns in surface waters of the World Ocean. *Deep-Sea Res.* **49,** 463–507 (2002).
11. Watson, A. J. *The Biogeochemical Cycle of Iron in Seawater* (John Wiley, 2001) Ch. 2.
12. De Baar, H. J. W. *et al.* Importance of iron for plankton blooms and carbon-dioxide drawdown in the Southern-Ocean. *Nature* **373,** 412–415 (1995).
13. Toggweiler, J. R. & Russell, J. Ocean circulation in a warming climate. *Nature* **451,** 286–288 (2008).
14. Boyd, P. W. *et al.* Microbial control of diatom bloom dynamics in the open ocean. *Geophys. Res. Lett.* **39,** L18601 (2012).
15. Frew, R. D. *et al.* Particulate iron dynamics during FeCycle in subantarctic waters southeast of New Zealand. *Glob. Biogeochem. Cycles* **20,** GB1S93 (2006).
16. Bowie, A. R. *et al.* Biogeochemical iron budgets of the Southern Ocean south of Australia: Decoupling of iron and nutrient cycles in the subantarctic zone by the summertime supply. *Glob. Biogeochem. Cycles* **23,** GB4034 (2009).
17. Boyd, P. W. *et al.* FeCycle: Attempting an iron biogeochemical budget from a mesoscale SF6 tracer experiment in unperturbed low iron waters. *Glob. Biogeochem. Cycles* **19,** GB4S20 (2005).
18. Croot, P. L. *et al.* Physical mixing effects on iron biogeochemical cycling: FeCycle experiment. *J. Geophys. Res.* **112,** C06015 (2007).
19. Johnson, K. S., Gordon, R. M. & Coale, K. H. What controls dissolved iron concentrations in the world ocean? *Mar. Chem.* **57,** 137–161 (1997).
20. Sallée, J-B., Speer, K., Rintoul, S. & Wijffels, S. Southern Ocean thermocline ventilation. *J. Phys. Oceanogr.* **40,** 509–529 (2010).
21. Law, C. S. Vertical eddy diffusion and nutrient supply to the surface mixed layer of the Antarctic Circumpolar Current. *J. Geophys. Res.* **108,** 3272 (2003).
22. Cisewski, B., Strass, V. H. & Prandke, H. Upper-ocean vertical mixing in the Antarctic Polar Front Zone. *Deep-Sea Res.* **52,** 1087–1108 (2005).
23. Wu, L., Jing, Z., Riser, S. & Visbeck, M. Seasonal and spatial variations of Southern Ocean diapycnal mixing from Argo profiling floats. *Nature Geosci.* **4,** 363–366 (2011).
24. Frants, M. *et al.* Analysis of horizontal and vertical processes contributing to natural iron supply in the mixed layer in southern Drake Passage. *Deep-Sea Res. II* **90,** 68–76 (2013).
25. Ellwood, M. J., Boyd, P. W. & Sutton, P. Winter-time dissolved iron and nutrient distributions in the Subantarctic Zone from 40–52S; 155–160E. *Geophys. Res. Lett.* **35,** L11604 (2008).
26. Wagener, T., Guieu, C., Losno, R., Bonnet, S. & Mahowald, N. Revisiting atmospheric dust export to the Southern Hemisphere ocean: Biogeochemical implications. *Glob. Biogeochem. Cycles* **22,** GB2006 (2008).
27. Lannuzel, D. *et al.* Distribution of dissolved iron in Antarctic sea ice: Spatial, seasonal, and inter-annual variability. *J. Geophys. Res.* **115,** G03022 (2010).
28. Lin, H., Rauschenberg, S., Hexel, C. R., Shaw, T. J. & Twining, B. S. Free-drifting icebergs as sources of iron to the Weddell Sea. *Deep-Sea Res. II* **58,** 1392–1406 (2011).
29. Raiswell, R., Benning, L. G., Tranter, M. & Tulaczyk, S. Bioavailable iron in the Southern Ocean: the significance of the iceberg conveyor belt. *Geochem. Trans.* **9,** 7 (2008).
30. Gerringa, L. J. A. *et al.* Iron from melting glaciers fuels the phytoplankton blooms in Amundsen Sea (Southern Ocean): Iron biogeochemistry. *Deep-Sea Res. II* **71–76,** 16–31 (2012).
31. Nishioka, J., Ono, T., Saito, H., Sakaoka, K. & Yoshimura, T. Oceanic iron supply mechanisms which support the spring diatom bloom in the Oyashio region, western subarctic Pacific. *J. Geophys. Res.* **116,** C02021 (2011).
32. Sarthou, G. *et al.* The fate of biogenic iron during a phytoplankton bloom induced by natural fertilisation: Impact of copepod grazing. *Deep-Sea Res. II* **55,** 734–751 (2008).
33. Strzepek, R. F. *et al.* Spinning the 'Ferrous Wheel': The importance of the microbial community in an iron budget during the FeCycle experiment. *Glob. Biogeochem. Cycles* **19,** GB4S26 (2005).
34. Sunda, W. G. & Huntsman, S. A. Iron uptake and growth limitation in oceanic and coastal phytoplankton. *Mar. Chem.* **50,** 189–206 (1995).
35. Marchetti, A. *et al.* Ferritin is used for iron storage in bloom-forming marine pennate diatoms. *Nature* **457,** 467–470 (2009).
36. Arrigo, K. R., van Dijken, G. L. & Bushinsky, S. Primary production in the Southern Ocean, 1997–2006. *J. Geophys. Res.* **113,** C08004 (2008).
37. Mackie, D. S. *et al.* Biogeochemistry of iron in Australian dust: From eolian uplift to marine uptake. *Geochem. Geophys. Geosys.* **9,** Q03Q08 (2008).
38. Gaiero, D. M., Probst, J. L., Depetris, P. J., Bidart, S. M. & Leleyter, L. Iron and other transition metals in Patagonian riverborne and windborne materials: Geochemical control and transport to the southern South Atlantic Ocean. *Geochim. Cosmochim. Acta* **67,** 3603–3623 (2003).
39. Stammerjohn, S., Massom, R., Rind, D. & Martinson, D. Regions of rapid sea ice change: An inter-hemispheric seasonal comparison. *Geophys. Res. Lett.* **39,** L06501 (2012).
40. Dierssen, H. M. Perspectives on empirical approaches for ocean color remote sensing of chlorophyll in a changing climate. *Proc. Natl Acad. Sci. USA* **107,** 17073–17078 (2010).
41. Lovenduski, N. S. & Gruber, N. Impact of the Southern Annular Mode on Southern Ocean circulation and biology. *Geophys. Res. Lett.* **32,** L11603 (2005).
42. Séférian, R. *et al.* Skill assessment of three earth system models with common marine biogeochemistry. *Clim. Dynam.* **40,** 2549–2573 (2012).
43. Steinacher, M. *et al.* Projected 21st century decrease in marine productivity: a multi-model analysis. *Biogeosciences* **7,** 979–1005 (2010).
44. Misumi, K. *et al.* The iron budget in ocean surface waters in the 20th and 21st centuries: projections by the Community Earth System Model version 1. *Biogeosci. Discuss.* **10,** 8505–8559 (2013).
45. Marinov, I., Doney, S. C. & Lima, I. D. Response of ocean phytoplankton community structure to climate change over the 21st century: Partitioning the effects of nutrients, temperature and light. *Biogeosciences* **7,** 3941–3959 (2010).
46. Henson, S., Cole, H., Beaulieu, C. & Yool, A. The impact of global warming on seasonality of ocean primary production. *Biogeosciences* **10,** 4357–4369 (2013).
47. Sallee, J. B., Wienders, N., Speer, K. & Morrow, R. Formation of subantarctic mode water in the southeastern Indian Ocean. *Ocean Dynam.* **56,** 525–542 (2006).
48. De Boyer Montegut, C., Madec, G., Fischer, A. S., Lazar, A. & Iudicone, D. Mixed layer depth over the global ocean: An examination of profile data and a profile-based climatology. *J. Geophys. Res.* **109,** C12003 (2004).
49. Strzepek, R. F., Maldonado, M. T., Hunter, K. A., Frew, R. D. & Boyd, P. W. Adaptive strategies by Southern Ocean phytoplankton to lessen iron limitation: Uptake of organically complexed iron and reduced cellular iron requirements. *Limnol. Oceanogr.* **56,** 1983–2002 (2011).

Acknowledgements

We thank all observational scientists that generously shared iron data (especially M. Klunder and P. Sedwick, who did so before publication), the GEOTRACES programme (www.geotraces.org), K. Arrigo and G. van Dijken for providing iron utilization data files and A. Barton for comments on the manuscript. The Argo float data were collected and made freely available by the International Argo Program (http://www.argo.ucsd.edu). This work benefitted from the support of the French Agence Nationale de la Recherche (ANR) grant ANR-10-LABX-18-01 of the national Programme Investissements d'Avenir, the CSIR Parliamentary Grant, NRF-SANAP and the EU FP7 Marie Curie International Research Staff Exchange Scheme (IRSES) Fellowship SOCCLI (The role of Southern Ocean Carbon cycle under CLImate change), which received funding from the European Commission's Seventh Framework Programme under grant agreement 317699. J.B.S. received support from Agence Nationale de la Recherche (ANR), ANR-12-PDOC-0001, as well as from the British Antarctic Survey as a BAS Fellow. This research was partly supported by the Australian Government Cooperative Research Centres Programme through the Antarctic Climate and Ecosystems CRC (ACE CRC), University of Tasmania Rising Stars grant no B0019024 and Australian Antarctic Science project no 2900, the New Zealand Ministry for Science and Innovation and the Institute of Marine and Antarctic Studies, University of Tasmania.

Author contributions

Led design of the study and writing of the manuscript (A.T.), assembly of the iron and Argo datasets and data analysis (A.T. and J-B.S.), additional physical flux analyses (A.T., J-B.S., M.L. and S.S.), biological rate measurements (P.W.B.) and additional iron observations (A.R.B.). All authors contributed to the overall experimental work, discussion of the results and their implications, as well as commenting on the manuscript.

Additional information

Supplementary information is available in the online version of the paper. Reprints and permissions information is available online at www.nature.com/reprints. Correspondence and requests for materials should be addressed to A.T.

Competing financial interests

The authors declare no competing financial interests.